ChemComm
Chemical Communications

Accepted Manuscript

This article can be cited before page numbers have been issued, to do this please use: X. Mao, A. Martinez, W. Samantha, S. Zou and J. He, *Chem. Commun.*, 2026, DOI: 10.1039/D6CC03058K.

ROYAL SOCIETY OF CHEMISTRY

rsc.li/chemcomm

ChemComm

View Article Online
DOI: 10.1039/D6CC03058K

COMMUNICATION

Chiroptical Modulation of Gold Nanorods by Self-Assembly: End-to-End vs. Side-by-Side

Xi Mao,[a] Abrahan Martinez,[c] Samantha Williams,[b] Shenli Zou,*[c] Jie He,*[a,b]

Received 00th January 20xx,
Accepted 00th January 20xx

DOI: 10.1039/x0xx00000x

We report polymer-guided assembly of chiral gold nanorods (AuNRs) into end-to-end (EE) and side-by-side (SS) modes, modulating their chiroptical responses. EE assemblies amplify circular dichroism (CD) response due to the interparticle plasmonic coupling along the continuously helical patterns of c-AuNRs along the chain direction, while SS assemblies reduce CD response as a result of racemic twisting.

Chiral plasmonic nanoparticles (NPs) are unique nanostructures with potential applications in chiroptical devices,[1, 2] chiral sensors,[3-5] biological applications[6-8] and asymmetric catalysis.[9-12] Synthesis of chiral NPs often involves a chiral ligand that promotes symmetry breaking during seed-mediated growth,[13, 14] thereby transferring molecular chirality to structural asymmetry with plasmonic chiroptical signals. Other than synthesizing discrete nanostructures with intrinsic chirality, the molecular asymmetry can be transferred by incorporating achiral NPs with chiral inducers, such as proteins, DNA, and amino acids.[15-20] Assemblies of achiral gold nanorods (AuNRs) with bovine serum albumin (BSA) formed right-handed twisted assemblies to enhance and amplify chiroptical response and produced circular dichroism (CD) asymmetry factor (*g*-factor) of 0.014.[21-24] AuNRs templated on amyloid fibers in end-to-end (EE) fashions showed an *g*-factor enhancement by more than 4600-fold.[25] On the other hand, chiroptical resonance can be controlled by designing the assemblies of chiral AuNRs (c-AuNRs).[26-28] Side-by-side (SS) assemblies obtained by structural self-matching assembly of c-AuNRs yield a 100-fold enhancement in *g*-factor, compared with individual c-AuNRs.[29] Single-particle CD spectroscopy further suggests that different assembly configurations, such as EE and SS, have distinct effects on chiroptical responses of AuNRs depending on interparticle distance and NP size.[30] Despite these advances in spectroscopic characterization, precise control over the solution self-assembly of chiral plasmonic NPs remains challenging. Herein, we report a self-assembly strategy for c-AuNRs using achiral polymer ligands and demonstrate the chiroptical modulation through assembly modes and interparticle plasmon coupling. Achiral AuNRs with two polystyrene (PS) domains at the two ends are used as, i) seeds to grow c-AuNRs in the presence of L- or D-cysteine (L-/D-cys) and further drive self-assembly along the lateral surface in an SS fashion; and ii) building blocks to construct nanorod chains and further grow as chiral chains.[31] This allows us to compare the impact of interparticle self-assemblies on their chiroptical resonance. The *g*-factor of c-AuNR EE assemblies is about twice that of discrete c-AuNRs. In contrast, the SS assembly formed from racemic twists exhibits a chiroptical signal reduced to about 50% of that of individual AuNRs. With natural proteins, e.g., BSA, the right-handed SS assemblies were also constructed via using electrostatic interaction, which enhanced chiroptical response by 4- to 12-fold for L- and D-chiral AuNRs, respectively.

AuNRs (100×18 nm) capped with cetyltrimethylammonium chloride (CTAC) were synthesized using a previously reported method by Murray's group (**Fig. S1**).[32] Surface modification was carried out in a DMF/water (100:1, vol) mixture containing thiol-terminated polystyrene (PS_{161}-SH, M_n = 16.8 kDa, PDI = 1.3) and polystyrene-*block*-poly (ethylene oxide) (PS_{37}-*b*-PEO_{140}, M_n = 10 kDa, PDI = 1.2). Typically, ~20 µL of concentrated AuNRs were injected into 2 mL of DMF solution containing PS_{161}-SH and PS_{37}-*b*-PEO_{140}. After incubating for 4 h, water was added to 15 vol%. The solution mixture was annealed at 90 ℃ for 30 min prior to purification by centrifugation. As PS_{161}-SH concentration ($C_{PS161\text{-}SH}$) decreased from 10 to 0.01 µM, the longitudinal localized surface plasmon resonance (LSPR) peak of AuNRs blue-shifted from 1006 to 880 nm (**Fig. S2a, b**), which was attributed to the slight deformation of AuNRs (length shortening to ~90 nm). At $C_{PS161\text{-}SH}$ of 10 µM, AuNRs were uniformly coated by PS with a polymer layer thickness of 16.8 ± 2.6 nm (**Fig. S3a, d**). Then, the PS thickness slightly decreased to 11.7 ± 2.8 nm as the PS concentration decreased to 1 µM. This decrease is attributed to the change of chain stretching status of PS_{161}-SH, further leading

[a] *Polymer Program, Institute of Materials Science, University of Connecticut, Storrs, Connecticut 06269, USA*
[b] *Department of Chemistry, University of Connecticut, Storrs, Connecticut 06269, USA*
[c] *Department of Chemistry, University of Central Florida, Orlando, Florida 32816, USA*
* *Email: shengli.zou@ucf.edu and jie.he@uconn.edu*

View Article Online
DOI: 10.1039/D6CC03059K

to the surface dewetting as reported previously.[31] TEM reveals the transition from core-shell AuNRs@PS to dumbbells (**Fig. S2c-j**), known as the surface dewetting under the deficient ligand condition of PS_{161}-SH.[31] With $C_{HS\text{-}PS161}$ in the range of 0.25 to 0.1 μM, dumbbell-like AuNRs with PS domains capped at the two ends were obtained (**Fig. S2g, h**). Thermogravimetric analysis (TGA) indicated the grafting densities (б) of PS_{161}-SH was 0.058 chains/nm^2 at $C_{PS161\text{-}SH}$ of 0.1 μM (**Fig. S4**), close to the critical grafting density as reported previously.[31, 33-35] The PS domains are 12.8 ± 2.3 nm at $C_{HS\text{-}PS161}$ of 0.1 μM and the yield of dumbbell-like AuNRs is >90% (**Fig. S3b-d**). Further decreasing $C_{PS161\text{-}SH}$ to 0.05 and 0.01 μM, the domain size became smaller to 8.9 ± 2.1 nm (**Fig. S2i, j**).

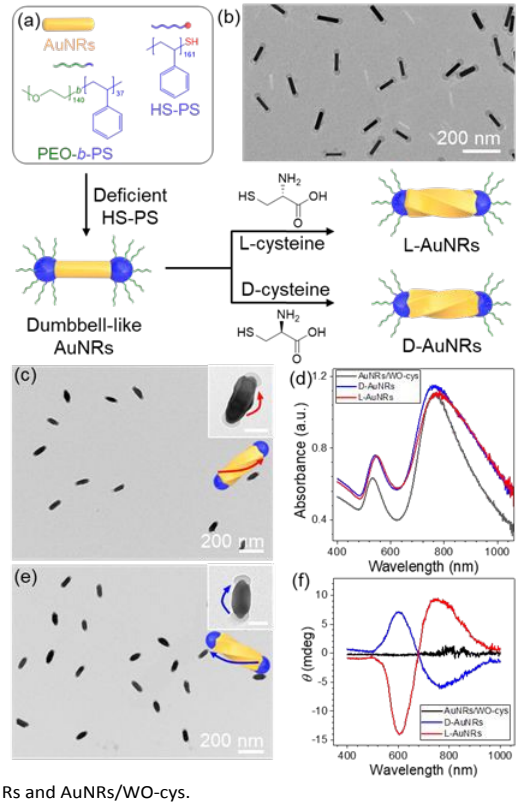

Fig. 1 (a) Scheme for the preparation of dumbbell-like AuNRs and c-AuNRs by seed-mediated growth. TEM images of AuNRs (b), L-AuNRs (c) and D-AuNRs (e). Scale bars of the inset images in (c, e) are 50 nm. UV-vis (d), and CD (f) spectra of L-/D-AuNRs and AuNRs/WO-cys.

c-AuNRs were synthesized via seed-mediated growth using dumbbell-like AuNRs as seeds in the presence of L-/D-cysteine (L-/D-cys) as chiral inducers (**Fig. 1a**).[29] With PS-capped AuNRs, chiral features grew along the lateral facets. This growth increased the diameter and caused the LSPR band to blue-shift to ~760 nm (**Fig.s 1b-e** and **S5**). As shown in TEM images, c-AuNRs with L-/D-cys, labelled as L-AuNRs and D-AuNRs, showed right-/left-handed helices as well as their average diameters increased to 38.6 ± 6.7 nm and 40.9 ± 6.2 nm after 8th growth, respectively (**Fig. 1b, e**). The L-/D-AuNRs exhibited clear, mirror-symmetric CD spectra, showing a transverse surface plasmon resonance (TSPR) band at 600 nm and a LSPR band at 760 nm, respectively (**Fig. 1f**). For L-AuNRs displayed a positive cotton effect at 756 nm and a negative cotton effect at 603 nm, while D-AuNRs showed the opposite peaks at the same positions. As a control, AuNRs grown without (WO-) L-/D-cys showed no CD response in the same range. The plasmonic CD originates from chiral surface distortion caused plasmonic harmonics.[36] The corresponding *g*-factor spectra of L-/D-AuNRs also showed symmetric signals with maximum *g*-factors at TSPR (603 nm) of -7.1×10^{-4} and 3.7×10^{-4} (**Fig. S6** and batch 1 in **Table S1**), respectively. Meanwhile, the diameter and CD intensities of c-AuNRs can be modulated by growth cycles. As growth cycle increased from 4 to 12, the diameter of L-AuNRs increased to 48.3 ± 6.9 nm (**Fig. S7a-c**). The increased diameter caused the TSPR band blue-shifted 540 nm (**Fig. S7d**); meanwhile, the *g*-factors gradually increased to -1.9×10^{-3} at ~530 nm (**Fig. S7e** and summarized in **Table S1**).

Similar seed-mediated growth strategy can be extended to AuNR chains. We prepared achiral AuNR chains by adding AuNRs into a DMF/water mixture containing PS_{161}-SH (1 μM) and PS_{37}-*b*-PEO_{140} (0.5 mg/mL) where the water content was set to 3.8 vol%, close to the critical water concentration of PS (~4.0 vol% for 1 μM PS solution in DMF).[37] The reduced solvent quality of PS ligands in water/DMF mixtures drove the end-to-end (EE) assembly of AuNRs, leading to the formation of achiral AuNRs chains (**Fig. 2b, c**). The nanorod chain length is 578 ± 220 nm (about 6-10 nanorods per chains). Meanwhile, the LSPR band red-shifted from 913 nm to 1145 nm. Using AuNR chains as seeds, the helices were grown with L-/D-cys, denoted as L-/D-Chains. After growth, the LSPR peak of chains red-shifted to 1235 nm (**Fig. 2j**). This ref-shift is likely due to the formation of epiphysis-like nanostructures on individual nanorods, that further enhances the interparticle plasmon coupling. TEM and SEM images suggested that L-/D-Chains were composed of c-AuNRs with right-/left handedness (**Fig. 2d-g**), respectively. Their average diameters (short axis of AuNRs) of L-/D-Chains were 27.7 ± 3.5 and 26.7 ± 3.3 nm, respectively. Compared with the *g*-factor of individual L-AuNRs at TSPR peak (520 nm) after 4th growth (-2.1×10^{-4}, **Fig. S7e**), the *g*-factor of L-Chains at TSPR peak (618 nm) increased to -5.5×10^{-4}, corresponding to 2.6 times of that of the individual L-AuNRs (**Fig. 2k, l**). To verify the impact of plasmon coupling on chiroptical properties, chiral AuNR chains were disassembled into discrete c-AuNRs by redispersing in DMF, a good solvent for PS (**Fig. 2h, i**). The LSPR peak blue-shifted from 1213 nm to 895 nm, confirming the disassembly of L-/D-Chains (**Fig. 2j**). The CD spectra of individual c-AuNRs collected in DMF showed the decrease of CD response after disassembly (**Fig. 2k**). The *g*-factor of L-Chains is 2 times, while the *g*-factor of D-Chains is 1.5 times, as compared to their discrete c-AuNRs (**Fig. 2l**). The enhanced *g*-factor originates from the synergistic effects of plasmonic coupling and the continuous helical organization of c-AuNRs. The red-shifted LSPR band indicates the formation of collective plasmon excitations, while the extended chiral geometry promotes their coherent chiroptical response, resulting in amplified CD intensity.[23, 38-40]

Furthermore, the CD response of AuNR chains is dependent on the number of growth cycles. As increasing the growth cycles to 8 or 12 resulted in the further red-shift of the LSPR to 1250 nm while transverse peak red-shifted to ~560 nm (**Fig. S8a**). TEM images showed a progressive diameter increase to 39 nm after the 12th growth (**Fig. S8c-j**). After 12th growth, the *g*-factor of L-Chains increased to -3.3×10^{-3} (**Fig. S8b and S9**), close to 5.8 times as compared to chains with 4th growth, and about 1.7 times of individual NRs (L-AuNRs with 12th growth, **Table S1**). Those helical spikes appeared to be periodic along the chain. Note that, the overgrowth on NR chains can result in the interconnection of NRs, i.e., the diameter of AuNRs become greater than that of polymers; after the 8th growth, the chains cannot be disassembled in DMF.

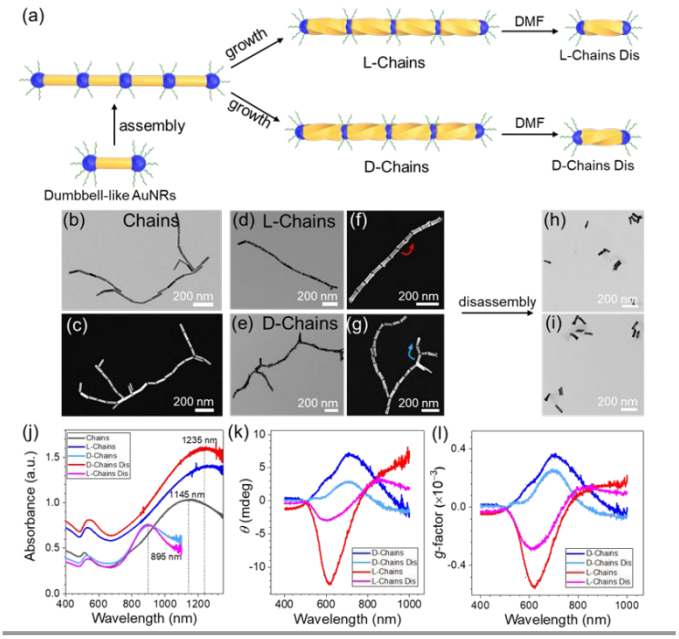

Fig. 2 (a) Scheme for the preparation of chiral AuNR chains by end-to-end (EE) and disassembly of chiral chains. TEM images of AuNR chains (b), chiral AuNR chains with L-cys (L-Chains) (d) and D-cys (D-Chains) (e). SEM images of AuNR chains (c), L-Chains (f) and D-Chains (g). (h, i) Individual c-AuNRs obtained by disassembly of L-/D-Chains: L-chains (h), D-chains (i). UV-vis (j), CD (k) and *g*-factor (l) of L-/D-Chains and disassembled NRs.

On the other hand, c-AuNRs can assemble in a twisted SS fashion.[41] The SS self-assembly of c-AuNRs were constructed by using methanol (MeOH) to disrupt the CTAC bilayer and drive the interaction of lateral surface of c-AuNRs (**Fig. 3a**). In a water/MeOH mixture (1/9, vol), the LSPR band of c-AuNRs showed a ~60 nm red shift after 2 h (**Fig. 3b**), similar to the reported value.[29] The CD spectra also displayed the red-shifted LSPR band (**Fig. S9**). TEM reveals that SS assemblies comprise of twisted but elongated c-AuNR clusters because of the steric repulsion among polymer domains at two ends of c-AuNRs. The size of SS assemblies grew and a red-shift of its longitudinal peak was observed later. Meanwhile, the CD response of SS assemblies decreased compared with individual c-AuNRs. The *g*-factor of L-AuNR SS assemblies at 829 nm decreased by 68%, while that at 604 nm decreased by 42%. Similarly, the intensity of D-AuNR SS assemblies at 829 nm decreased by 63%, and that at 604 nm decreased by 39% (**Fig. 3e**). The reduced chiroptical response in the SS assembly, likely attributed to the racemic twisting within individual assemblies, i.e., the coexistence of both left-/right-handed twist in one single assemblies.

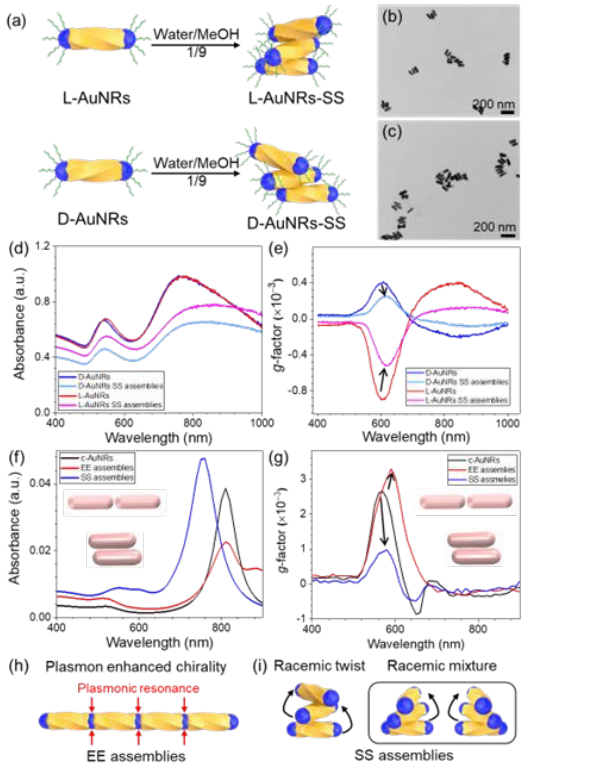

Fig. 3 Side-by-side (SS) assembly of c-AuNRs in water/MeOH (volume ratio: 1/9): scheme (a), UV-vis spectra (b), TEM images of SS assemblies of L-AuNRs (c) and D-AuNRs (d) and *g*-factor spectra (e). Simulated UV-vis (f), *g*-factor (g) spectra, and (h, i) schematic illustration of c-AuNR EE and SS assemblies. The insets in Fig. 3f, g are snapshots of EE and SS assemblies.

To gain further insight into chiroptical modulation via assembly modes, we used the discrete dipole approximation (DDA) method to simulate the impact of chiral SS and EE assemblies on the *g*-factors. The chiral AuNRs (100 nm×30 nm) used for simulation have chiral curls with a width of approximately 3 nm and a height of 2 nm. The structural configurations were not intended to exactly reproduce the experimental configuration; rather, they were chosen to ensure the stability of the calculated g-factor and to examine the effects of the SS and EE assemblies on the g-factor in comparison to a single c-AuNRs. The UV-vis spectra showed a blue shift for SS assemblies and red shift for EE assemblies (**Fig. 3f**), compared with individual c-AuNR. The *g*-factor spectra indicated a ~1.6-fold decrease for SS assemblies and a 0.3-fold enhancement for EE assemblies (**Fig. 3g**), relative to individual c-AuNR, consistent with experimental results. We note that the periodicity of surface chiral features is of key importance for this enhancement. In the EE assemblies, the rotation of individual c-AuNRs without periodical chiral structures would lead to the loss of the *g*-factor. Therefore, the enhanced chiroptical response of the EE assemblies is likely due to continuous dissymmetrical electric field distribution along the longitudinal direaction.[42, 43] In contrast, the reduced chiroptical signals observed for the SS assemblies are attributed to racemic twists that cancel the overall chirality (**Fig. 3i**).[41, 44] Because the SS oligomers exhibit direct plasmonic coupling of

the TSPR mode, stronger coupling is expected to exert a greater influence on their chiroptical signals, as demonstrated by Wang et al.[30]

To support this hypothesis, we further use BSA which is negatively charged to induce the single-handed SS assemblies of c-AuNRs.[20, 24] L-/D-AuNRs with diameter of 44.4 ± 7.2 nm and 39.2 ± 5.6 nm, respectively (**Fig. S10a, b**), were mixed with BSA at a concentration of 1 μM in 1 mM PBS buffer (pH = 6.4). The polymer domains at the two ends of c-AuNRs suppress EE assembly, while the asymmetric chiral surface-charge distribution of BSA electrostatically guides neighboring c-AuNRs into a preferred handed twist. The red shift of the LSPR band of c-AuNRs was about 15 nm after 90 min (**Fig. 4b**). TEM images suggested that the SS assemblies were composed of two or three twisted c-AuNRs (**Fig. 4c, d**). Correspondingly, the CD intensities showed a significant enhancement (**Fig. S10c, d**). Compared with individual c-AuNRs, the *g*-factor at 660 nm of D-AuNRs increased by 12.4 times, while that of L-AuNRs increased by 4 times (**Fig. 4e**). This enhancement is attributed to the formation of right-handed helices in the presence of BSA.

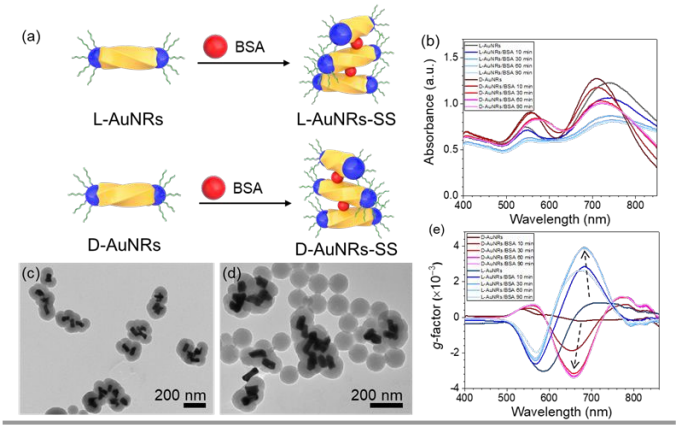

Fig. 4 BSA-induced SS assembly of c-AuNRs: Scheme (a), UV-vis spectra (b), TEM images of SS assemblies of L-AuNRs (c), D-AuNRs (d) after silica coating and *g*-factor spectra (e).

In summary, we demonstrate a chiroptical modulation strategy by controlling the assembly modes of chiral AuNRs: end-to-end (EE) and side-by-side (SS). Our results revealed that the periodic continuous dissymmetrical features in EE assemblies exhibit chiral enhancements, doubling the CD signals. In contrast, SS assemblies decrease the chiral signals compared with individual c-AuNRs, reducing CD intensity to approximately half in the LSPR region and by about 0.6-fold in the TSPR region, due to the formation of racemic twist. BSA-induced right-handed SS assemblies increase CD signals by 4- to 12-fold because of the decrease of racemic twist and racemic mixture. These findings highlight the critical role of assembly modes in the chiroptical properties of chiral NPs, offering a versatile route to achieve chiroptical modulation. The amplified CD response of EE assemblies may enable sensitive chiroptical detection of stereoisomeric drugs, through CD signal changes induced by drug-polymer interactions.[45]

Author contributions

X. Mao: Methodology, Investigation, Formal analysis, Writing – original draft, Writing – review & editing; A. Martinez: Software, Formal analysis, Review & editing; S. Williams: Investigation, Review & editing; S. Zou: Software, Supervision, Formal analysis, Funding acquisition, Writing – review & editing; J. He: Conceptualization, Supervision, Project administration, Funding acquisition, Writing – review & editing.

Conflicts of interest

There are no conflicts to declare.

Data availability

Electronic supplementary information (ESI) available. Experimental procedures: synthesis of AuNRs, dumbbell-like AuNRs and chains, self-assembly of chiral AuNRs; characterization methods; TGA curves, additional TEM and SEM images, analysis, UV-vis and CD absorption spectra. See DOI: XXX.

Acknowledgements

JH acknowledges the financial support from USDA National Institute of Food and Agriculture, AFRI 392 project (proposal number 2022-08607). SZ thanks the support from National Science Foundation under collaborative Award No. CBET-2230729 & 2230891. We are also grateful for the partial support from the University of Connecticut through its Research Excellence Program (REP).

Notes and references

1 L. A. Warning, A. R. Miandashti, L. A. McCarthy, Q. Zhang, C. F. Landes and S. Link, ACS Nano, 2021, 15, 15538-15566.
2 J. Zheng, Y. Fu, J. Wang, W. Zhang, X. Lu, H.-Q. Lin, L. Shao and J. Wang, Nat. Commun., 2025, 16, 1658.
3 C. Hao, D. Meng, W. Shi, C. Xu, Q. Wang and H. J. A. C. Kuang, Angew. Chem. Int. Ed., 2025, 137, e202502115.
4 A. Serrano-Freijeiro, M. Zarzuela-Amor, C. Renero-Lecuna, M. Obelleiro-Liz, V. F. Martín, I. Pérez-Juste, J. M. Taboada, J. Casado, I. Pastoriza-Santos, J. Pérez-Juste, S. Bals and L. M. Liz-Marzán, ACS Nanosci. Au, 2026, DOI: https://doi.org/10.1021/acsnanoscienceau.5c00184.
5 J. Cai, W. Zhang, L. Xu, C. Hao, W. Ma, M. Sun, X. Wu, X. Qin, F. M. Colombari, A. F. de Moura, J. Xu, M. C. Silva, E. B. Carneiro-Neto, W. R. Gomes, R. A. L. Vallée, E. C. Pereira, X. Liu, C. Xu, R. Klajn, N. A. Kotov and H. Kuang, Nat. Nanotechnol., 2022, 17, 408-416.
6 Z. Li, A. Qu, C. Xu, H. Kuang, L. Xu and M. Sun, Adv. Mater., 2025, 37, 2504458.
7 M. Lu, A. Qu, X. Huang, T. Shi, W. Chen, C. Xu, H. Kuang and G. Zhang, Acc. Chem. Res., 2025, 58, 2613-2626.
8 C. Hao, C. Xu and H. Kuang, Chem. Commun., 2023, 59, 12959-12971.
9 W. Fu, C. Tang and P. Wang, Adv. Mater., 2025, e15236, DOI: 15210.11002/adma.202515236.
10 Z. Wang, J. Wan, X. Sun, L. Sun, S. Chen and Q. Zhang, J. Am. Chem. Soc., 2025, 147, 15767-15776.
11 J. Dong, L. Xu, X. Xu, B. Shi, Q. Wang, J. Xu, C. Xu, H. Kuang and A. Qu, J. Am. Chem. Soc., 2026, 148, 3654-3671.

12 F. Wang, W. Yang, Q. Ding, X. Xing, L. Xu, H. Lin, C. Xu and S. Li, Angew. Chem. Int. Ed., 2025, 64, e202415031.
13 S. W. Im, D. Zhang, J. H. Han, R. M. Kim, C. Choi, Y. M. Kim and K. T. Nam, Nat. Mater., 2024, 23, 977-983.
14 H.-E. Lee, R. M. Kim, H.-Y. Ahn, Y. Y. Lee, G. H. Byun, S. W. Im, J. Mun, J. Rho and K. T. Nam, Nat. Commun., 2020, 11, 263.
15 X. Lan, Z. Chen, G. Dai, X. Lu, W. Ni and Q. Wang, J. Am. Chem. Soc., 2013, 135, 11441-11444.
16 W. Ma, H. Kuang, L. Xu, L. Ding, C. Xu, L. Wang and N. A. Kotov, Nat. Commun., 2013, 4, 2689.
17 Z. Cao, H. Gao, M. Qiu, W. Jin, S. Deng, K.-Y. Wong and D. Lei, Adv. Mater., 2020, 32, 1907151.
18 J. Kumar, H. Eraña, E. López-Martínez, N. Claes, V. F. Martín, D. M. Solís, S. Bals, A. L. Cortajarena, J. Castilla and L. M. Liz-Marzán, Proc. Natl. Acad. Sci. U. S. A., 2018, 115, 3225-3230.
19 F. Zhang, Y. Bi, J. Wei and Z. Yang, Chem. Commun., 2025, 61, 14087-14096.
20 J. Zhou, Y. Gao, D. Zhang, K. Ren, M. Dai, H. Wang and L. Qi, Nat. Commun., 2025, 16, 6897.
21 B. Han, Z. Zhu, Z. Li, W. Zhang and Z. Tang, J. Am. Chem. Soc., 2014, 136, 16104-16107.
22 G. Cheng, D. Xu, Z. Lu and K. Liu, ACS Nano, 2019, 13, 1479-1489.
23 J. Lu, Y.-X. Chang, N.-N. Zhang, Y. Wei, A.-J. Li, J. Tai, Y. Xue, Z.-Y. Wang, Y. Yang, L. Zhao, Z.-Y. Lu and K. Liu, ACS Nano, 2017, 11, 3463-3475.
24 Z.-Y. Wang, N.-N. Zhang, J.-C. Li, J. Lu, L. Zhao, X.-D. Fang and K. Liu, Soft Matter, 2021, 17, 6298-6304.
25 J. Lu, Y. Xue, K. Bernardino, N.-N. Zhang, W. R. Gomes, N. S. Ramesar, S. Liu, Z. Hu, T. Sun, A. F. de Moura, N. A. Kotov and K. Liu, Science, 2021, 371, 1368-1374.
26 S. Wang, X. Liu, S. Mourdikoudis, J. Chen, W. Fu, Z. Sofer, Y. Zhang, S. Zhang and G. Zheng, ACS Nano, 2022, 16, 19789-19809.
27 S. Maniappan, C. Dutta, D. M. Solís, J. M. Taboada and J. Kumar, Angew. Chem. Int. Ed., 2023, 62, e202300461.
28 H. Kang, Y. Jeon, K. Baek, S. Park, J. Lee, T. S. Shim, J. K. Hyun and S.-J. Park, Nat. Commun., 2025, 16, 7076.
29 N.-N. Zhang, M. Mychinko, S.-Y. Gao, L. Yu, Z.-L. Shen, L. Wang, F. Peng, Z. Wei, Z. Wang, W. Zhang, S. Zhu, Y. Yang, T. Sun, L. M. Liz-Marzán, S. Bals and K. Liu, Nano Lett., 2024, 24, 13027-13036.
30 L. Zhang, Y. Chen, J. Zheng, G. R. Lewis, X. Xia, E. Ringe, W. Zhang and J. Wang, Angew. Chem. Int. Ed., 2023, 62, e202312615.
31 H. Duan, Z. Jia, M. Liaqat, M. D. Mellor, H. Tan, M.-P. Nieh, Y. Lin, S. Link, C. F. Landes and J. He, ACS Nano, 2023, 17, 12788-12797.
32 X. Ye, C. Zheng, J. Chen, Y. Gao and C. B. Murray, Nano Lett., 2013, 13, 765-771.
33 R. M. Choueiri, E. Galati, H. Thérien-Aubin, A. Klinkova, E. M. Larin, A. Querejeta-Fernández, L. Han, H. L. Xin, O. Gang, E. B. Zhulina, M. Rubinstein and E. Kumacheva, Nature, 2016, 538, 79-83.
34 Z. Nie, D. Fava, E. Kumacheva, S. Zou, G. C. Walker and M. Rubinstein, Nat. Mater., 2007, 6, 609-614.
35 K. Liu, Z. Nie, N. Zhao, W. Li, M. Rubinstein and E. Kumacheva, Science, 2010, 329, 197-200.
36 Z. Fan and A. O. Govorov, Nano Lett., 2012, 12, 3283-3289.
37 L. Zhang, H. Shen and A. Eisenberg, Macromolecules, 1997, 30, 1001-1011.
38 K. Liu, A. Ahmed, S. Chung, K. Sugikawa, G. Wu, Z. Nie, R. Gordon and E. Kumacheva, ACS Nano, 2013, 7, 5901-5910.
39 Z. Fan and A. O. Govorov, Nano Letters, 2010, 10, 2580-2587.
40 L. Hu, T. Liedl, K. Martens, Z. Wang and A. O. Govorov, ACS Photonics, 2019, 6, 749-756.
41 K. W. Smith, H. Zhao, H. Zhang, A. Sánchez-Iglesias, M. Grzelczak, Y. Wang, W.-S. Chang, P. Nordlander, L. M. Liz-Marzán and S. Link, ACS Nano, 2016, 10, 6180-6188.
42 A. Lukach, K. Liu, H. Therien-Aubin and E. Kumacheva, J. Am. Chem. Soc., 2012, 134, 18853-18859.
43 A. F. Stewart, A. Lee, A. Ahmed, S. Ip, E. Kumacheva and G. C. Walker, ACS Nano, 2014, 8, 5462-5467.
44 Q. Zhang, T. Hernandez, K. W. Smith, S. A. Hosseini Jebeli, A. X. Dai, L. Warning, R. Baiyasi, L. A. McCarthy, H. Guo, D.-H. Chen, J. A. Dionne, C. F. Landes and S. Link, Science, 2019, 365, 1475-1478.
45 A. Biswas, P. Cencillo-Abad, M. W. Shabbir, M. Karmakar and D. Chanda, Sci. Adv., 2024, 10, eadk2560.

View Article Online
DOI: 10.1039/D6CC03058K

Data availability statements

Electronic supplementary information (ESI) available. Experimental procedures: synthesis of AuNRs, dumbbell-like AuNRs and chains, self-assembly of chiral AuNRs; characterization methods; TGA curves, additional TEM and SEM images, analysis, UV-vis and CD absorption spectra. See DOI: XXX.